A Novel Synchronous Phase Shifted PWM Strategy for Cascaded-H-Bridge-fed PMSM Drive

Gioacchino Scaglione
Department of Engineering
University of Palermo
Palermo, Italy
gioacchino.scaglione@unipa.it

Claudio Nevoloso
Department of Engineering
University of Palermo
Palermo, Italy
claudio.nevoloso@unipa.it

Giuseppe Schettino
Department of Engineering
University of Palermo
Palermo, Italy
giuseppe.schettino@unipa.it

Antonino Oscar Di Tommaso
Department of Engineering
University of Palermo
Palermo, Italy
antoninooscar.ditommaso@unipa.it

Rosario Miceli
Department of Engineering
University of Palermo
Palermo, Italy
rosario.miceli@unipa.it

***Abstract*—This paper proposes a novel synchronous phase shifted pulse width modulation strategy for a three-phase five level cascaded H-bridge multilevel inverter-fed permanent magnet synchronous machine drive. The key novelty of the proposed strategy deals with the adoption of the apparent switching frequency to identify a novel optimal frequency modulation index that guarantees voltages half-wave and three-phase symmetries, even if it is a non-integer number. Then, a novel optimal switching frequency-motor speed pattern is defined. The effectiveness of the proposed strategy is verified through experimental analysis, both in steady-state and dynamic working conditions.**

Keywords—Synchronous PWM, Cascaded H-Bridge, PMSM Drives, Field Oriented Control.

I. INTRODUCTION

Medium-Voltage (MV) drives play a crucial role in industrial automation by enabling precise and efficient control of large motors in energy-intensive sectors such as oil and gas, mining, metals, and water treatment [1]. According to [2], MV drive controllers must ensure low current harmonic distortion, low switching frequency, and fast current control dynamics. Multilevel inverters (MIs) are well-established technologies in these applications [3] since they mitigate issues related to switching and conduction losses due to reduced voltage stress on semiconductor devices. Among them, Cascaded H-Bridge Multilevel Inverter (CHBMI) represents the preferred choice due to its modularity and scalability that enable high-quality waveforms, fault tolerance, simplified maintenance, and high efficiency [4]-[5]. The performance of CHBMI-fed drives is highly dependent on the selected modulation and control techniques. In detail, Field Oriented Control (FOC) combined with Multi-Carrier Pulse Width Modulation (MC-PWM) is typically adopted since they strike a good balance between implementation complexity and performance [6]-[7]. Specifically, Phase Shifted (PS) MC-PWM is preferred for CHBMIs, as it shifts harmonics to the high-frequency range, allowing for lower switching frequencies ($\leq$ 500 Hz), and guaranteeing an equal power distribution among CHBMI sub-modules [8]. To further reduce harmonic distortion in very low switching frequency working conditions, Synchronous (Synch) and Optimal PWM techniques are typically adopted in MV drive applications [9]. Synch PWM is based on synchronization between the inverter switching frequency with the fundamental frequency to ensure half-wave and three-phase symmetries, effectively eliminating subharmonics. It can be easily implemented using standard modulation strategies with variable switching frequency capabilities. For two-Level Voltage Source Inverter (2L-VSI)-fed drives, extensive research [10]-[12] has demonstrated that half-wave and three-phase symmetries are ensured when the frequency modulation index is an odd integer multiple of three. Based on this principle, a switching frequency pattern can be defined as a function of rotor speed, enabling real-time frequency adaptation. Despite the extensive investigation in 2L-VSI applications, Synch PWM has received limited attention in the context of CHBMI-fed drives. The authors of [13] provide a generalized theory of PS-PWM strategy for CHBMIs and modular MIs. Particular attention is paid to the identification of the optimal phase shift among carriers. However, no attention is paid to the synchronization between carriers frequency and fundamental frequency. Authors of this work investigated the impact of the MC-PWM strategy on the CHBMI efficiency [14], PWM Multilevel Inverter-Driven IPMSM efficiency and motor energy class determination [15]. However, no attention has been paid to the optimal synchronization between carriers frequency and fundamental voltage frequency. Authors of [16] investigated the optimal synchronization between carriers frequency and fundamental frequency with the PS-PWM strategy, concluding that the inverter voltage waveform maintains three-phase and half-wave symmetry for carriers having $3k$ times the fundamental frequency, with k being any odd/even integer.

This work proposes a novel Synch-PS-PWM strategy for a CHBMI-fed PMSM drive. The key novelty of this work deals with adopting the apparent switching frequency to define the apparent frequency modulation index and investigate its impact on voltage and current spectra. Such an analysis allows for defining a novel optimal frequency modulation index m_f^* that guarantees half-wave and three-phase symmetries even if it is a non-integer number. Such a new parameter is finally adopted to define a novel optimal switching frequency-motor speed pattern. Experimental validation proves the effectiveness of the proposed novel Syn-PS-PWM strategy both in steady state and dynamic working conditions. The paper is structured as follows: Section II introduces the apparent frequency modulation index

and explores its impact on the phase voltage spectra; Section III describes the Synch PS-PWM-based FOC for three-Phase-five-Level-CHBMI (3P-5L-CHBMI) fed IPMSM drive; Section IV presents the test setup; Section V proves the effectiveness of the proposed control strategy in steady state and dynamic working conditions. Finally, Section VI presents the work conclusions.

II. Apparent Frequency Modulation Index: Definition and Properties

In this section, the main features of the adopted CHBMI topology and PS-PWM strategy are reported. Subsequently, the apparent switching frequency is introduced and adopted to define the apparent frequency modulation index and investigate its impact on the voltage spectra in the simulation environment.

A. Main features of the CHBMI topology and PS-PWM strategy

In this work, the IPMSM is fed by a PS-PWM-driven 3P-5L-CHBMI, whose circuit diagram and modulation scheme are reported in Fig. 1 and Fig. 2, respectively.

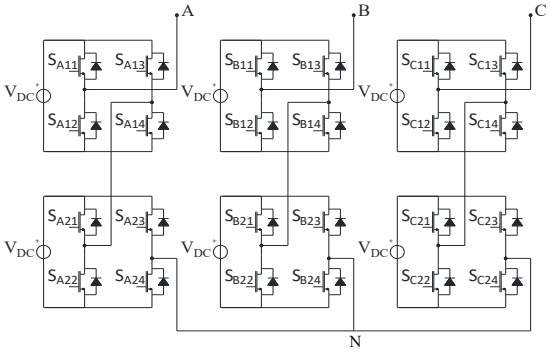

Fig. 1. 3P-5L CHBMI circuit diagram.

Fig. 2. Phase Shifted Pulse width Modulation scheme.

The CHBMI is an MI topology characterized by several H-Bridge (HB) modules connected in a cascaded fashion that can be controlled independently. Regarding the PS-PWM strategy, according to [14], carriers are characterized by the same peak-to-peak amplitude, the same average value equal to zero, and a mutual phase shift that depends on the number of cascaded HB modules per phase n_{HB}. In detail, the phase φ_i to assign to the i^{th} carrier is computed as follows:

$$\varphi_i = \frac{(i-1)\cdot\pi}{n_{HB}} \tag{1}$$

According to the modulation scheme shown in Fig. 2, each HB in the same phase is controlled with a classical Unipolar PWM strategy, and the related Gate Control Signals (GCSs) are phase-shifted by φ_i. Consequently, the carriers frequency f_c coincides with the switching frequency of each power switch f_{sw}.

In the frequency domain, phase voltage harmonics are centered around multiples of the switching frequency f_{sw} as a function of the number of inverter voltage levels n_l, according to the following relation:

$$f_h = j(n_l - 1)f_{sw}, \quad j \in \mathbb{N}^+ \tag{2}$$

In a 3P-5L CHBMI topology, harmonics are centered around $4f_{sw}$ and its multiples.

B. Definition of the apparent frequency modulation index

According to the standard approach adopted in the scientific literature [16], the frequency modulation index m_f is defined as:

$$m_f = \frac{f_{sw}}{f_1} \tag{3}$$

where f_{sw} is the switching frequency, and f_1 is the fundamental frequency, which is a function of the motor speed. According to [16], concerning the PS-PWM-driven CHBMI, to guarantee half-wave and three-phase symmetries in the voltage waveforms, m_f must be equal to $3k$, with $k \in \mathbb{N}^+$. In this way, even harmonics and multiples of three harmonics are null. However, the novel Synch-PS-PWM strategy proposed in this work exploits the PS-PWM strategy properties of shifting harmonics over the spectrum. Indeed, for a fixed switching frequency f_{sw} and fixed number of the CHBMI voltage levels n_l, modulation harmonics are grouped over the spectrum according to (2). Therefore, it is possible to define the apparent switching frequency $f_{sw,a}$ by fixing j=1, as follows:

$$f_{sw,a} = (n_l - 1) f_{sw} \tag{4}$$

Indeed, apparent switching frequency $f_{sw,a}$ identifies the first group of modulation harmonics over the spectrum and provides information about the equivalent switching frequency at the inverter output, which is correlated to the global converter switching losses. Then, it is possible to define an apparent frequency modulation index $m_{f,a}$ and investigate its impact on the voltage spectra. The apparent frequency modulation index $m_{f,a}$ can be defined as:

$$m_{f,a} = \frac{f_{sw,a}}{f_1} \tag{5}$$

It gives information about the equivalent number of switching pulses per fundamental period.

C. Analysis of the apparent frequency modulation index impact on the voltages spectra

To investigate the impact of the apparent frequency modulation index $m_{f,a}$ on the voltage spectrum, a simple mathematical model of the PS-PWM-driven 3P-5L CHBMI is implemented in the MATLAB environment. In detail, each power switch and its anti-parallel diode are modelled as an ideal bidirectional switch with zero switching time, and zero conduction and switching losses. Thus, it is possible to assign to each power switch a Boolean state variable $S_{j,xy} \in \{0, 1\}$, where $j \in \{A, B, C\}$ identifies the converter phase, $x \in \{1, 2\}$ identifies the considered HB per phase, and $y \in \{1, 4\}$ identifies the HB power switch. Moreover, considering that switches on the same HB leg must operate dually and in pairs to avoid the DC link short circuit, the HB leg state is automatically defined by considering only the state function of the upper power switch.

Therefore, the phase voltage v_{jN} is expressed in terms of the HB leg state function $S_{j,xy}$, and of the DC link voltage V_{DC} of each HB module as follows:

$$v_{jN} = V_{DC}(S_{j,11} - S_{j,13} + S_{j,21} - S_{j,23}) \quad (6)$$

The 3P-5L-CHBMI is analyzed in symmetrical configuration at no-load operating condition, assuming a constant DC-link voltage for each HB module. Such a simple mathematical model is adopted to investigate the phase voltages in the time and frequency domain for six different values of the apparent frequency modulation index, $m_{f,a} \in \{15, 16, 17, 17.5, 18, 24\}$, and simulation results are reported in Fig. 3. Looking at the simulation results, some considerations can be carried out and they are listed below:

- $m_{f,a} \in \mathbb{N}^+$ is an odd multiple of three (e.g., $m_{f,a}$=15, Fig. 3 (a)): voltage waveforms exhibit three-phase symmetry but lack half-wave symmetry. This is confirmed by the corresponding spectra, which are superimposed and include both odd and even harmonics; in particular, dominant harmonics, clustered around the apparent switching frequency, are even;
- $m_{f,a} \in \mathbb{N}^+$ is an even (e.g., $m_{f,a}$=16, Fig. 3 (b)): voltage waveforms exhibit half-wave symmetry but not three-phase symmetry. The associated spectra are not superimposed and contain only odd harmonics;
- $m_{f,a} \in \mathbb{N}^+$ is an odd not multiple of three (e.g., $m_{f,a}$=17, Fig. 3 (c)): voltage waveforms lack both three-phase symmetry and half-wave symmetry. However, the asymmetry among phases is less pronounced than in the case of $m_{f,a}$=16 (only harmonics of order higher than 40 are not superimposed), and the harmonics clustered around the apparent switching frequency are even;
- $m_{f,a} \in \mathbb{Z}$ (e.g., $m_{f,a}$=17.5, Fig. 3 (d)): voltage waveforms exhibit neither three-phase symmetry nor half-wave symmetry. The spectra exhibit a significant lack of symmetry, with the first group of harmonics including both odd and even components, representing the worst-case scenario;
- $m_{f,a} \in \mathbb{N}^+$ is an even multiple of three (e.g., $m_{f,a}$=18 and $m_{f,a}$=24, Fig. 3 (e) and (f), respectively): voltage waveforms exhibit both three-phase and half-wave symmetries. Spectra are superimposed and contain only odd harmonics, representing the best-case scenario.

According to the simulation results discussed so far, phase voltages exhibit half-wave and three-phase symmetries when $m_{f,a}$ is an even and multiple-of-three integer positive number. Thus, it is possible to define a novel optimal apparent frequency modulation index $m_{f,a}^*$ as follows:

$$m_{f,a}^* = 6k, \quad k \in \mathbb{N}^+ \quad (7)$$

Combining equations (3), (4), (5), and (7), a novel optimal frequency modulation index m_f^* is obtained:

$$m_f^* = \frac{6}{n_l - 1}k \quad k \in \mathbb{N}^+ \quad (8)$$

According to equation (8), the optimal value of the frequency modulation index depends on the number of CHBMI voltage levels. Moreover, the phase voltages half-wave and three-phase symmetries are guaranteed even if m_f^* is a fractional number, in contrast to the standard recommendations in the scientific literature [16]. Indeed, for a 3P-5L-CHBMI, m_f^*=3/2k. It must be underlined that, by defining k'=k/2, then m_f^*=3k'; when k is an even number, it results that m_f^* is an odd or even integer number multiple of three, falling within the set of modulation indices m_f recommended in [16], as it is highlighted in TABLE I. Such a statement is further proven by looking at the simulations results reported in Fig. 3 (e) and (f). Indeed, according to (8), the apparent frequency modulation indices $m_{f,a}$=18 and $m_{f,a}$=24 correspond to the frequency modulation indices m_f^*=4.5 and m_f^*=6. Although only m_f^*=6 falls within the set of modulation indices m_f recommended in [16], phase voltages exhibit the same behaviour in the frequency domain for both frequency modulation index values. Thus, it can be stated that the proposed optimal m_f^* not only includes the values of m_f recommended in [16] but extends the set of optimal modulation indices, effectively doubling the available value options.

III. Synchronous PS-PWM-Based Field Oriented Control for 3P-5L-CHBMI-fed IPMSM Drive

Given the results reported so far, this section proposes a novel Synch PS-PWM-based FOC for an IPMSM drive fed by the PS-PWM-driven 3P-5L-CHBMI with a novel switching frequency-motor speed pattern. The AC drive present at the Sustainable Development and Energy Saving Laboratory (SDESLAB) of the University of Palermo is adopted for this application. It consists of six MOSFET-based HB modules powered by six 55 V DC power supplies, and a 6-pole three-phase IPMSM whose technical data are reported in TABLE II.

TABLE I. Comparison Between Available Values of m_f According to [16] and to the Pattern Proposed in This Work.

k/2	m_f according to [16]	Novel optimal m_f^*
0.5	-	1.5
1	3	3
1.5	-	4.5
2	6	6
2.5	-	7.5
3	9	9
3.5	-	10.5
4	12	12
4.5	-	13.5
5	15	15

TABLE II: IPMSM Main Technical Data.

Quantity	Symbol	Value
Rated Voltage	V_{LL}	132 Vrms
Rated current	I_n	3.6 Arms
Rated Speed	n	4000 rpm
Nr. of pole pairs	P	3
Nr. of phases	m	3
Rated torque	T_{emn}	1.8 Nm

A. Design of a Novel Switching Frequency-Motor Speed Pattern

The novel switching frequency-motor speed pattern is designed based on the adopted IPMSM speed range (0-4000 rpm) and on the desired CHBMI switching frequency range. In detail, the adopted switching frequency range in this application is $f_{sw} \in \{550–750$ Hz$\}$, which is typical in industrial MV drives applications. Then, the IPMSM speed operative area is split into two ranges: for low-speed working conditions (n<500 rpm),

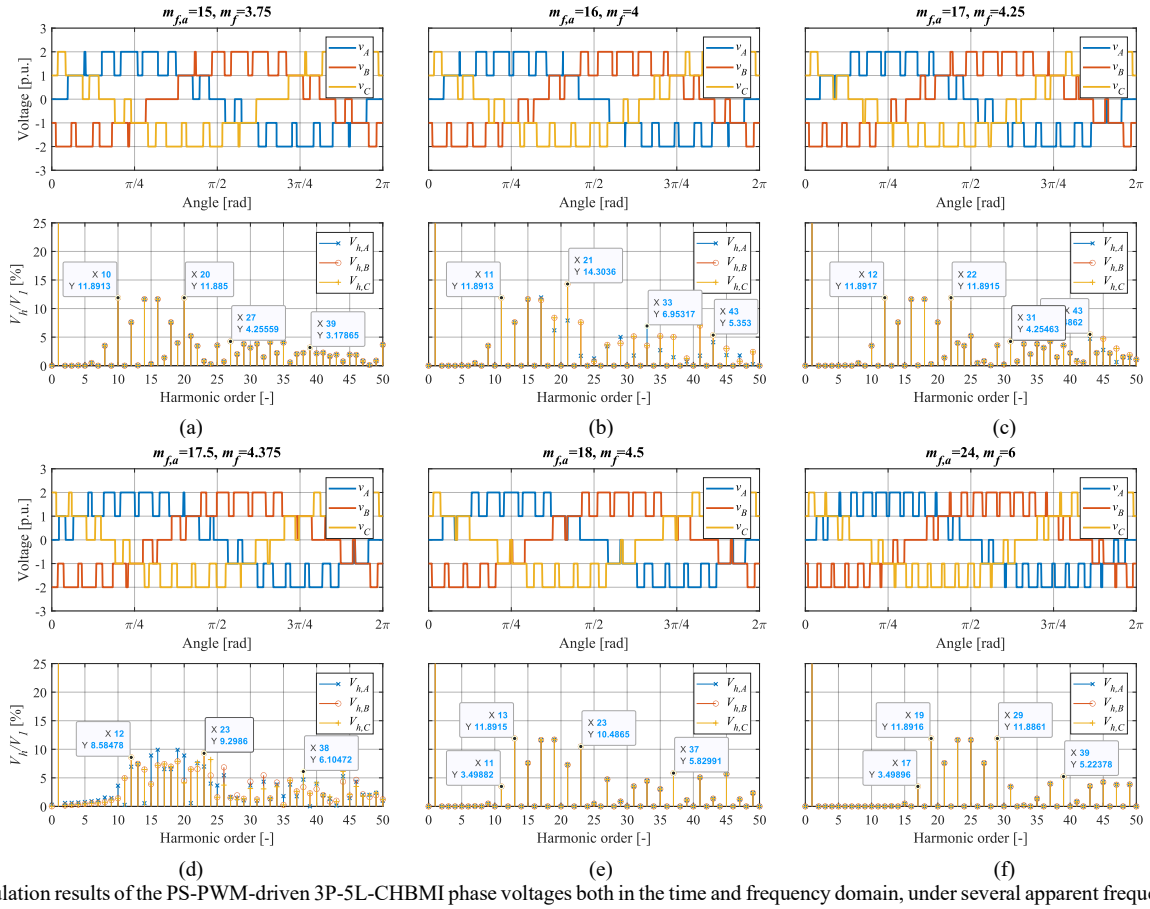

Fig. 3. Simulation results of the PS-PWM-driven 3P-5L-CHBMI phase voltages both in the time and frequency domain, under several apparent frequency modulation index values; (a) $m_{f,a}$=15, (b) $m_{f,a}$=15, (c) $m_{f,a}$=17, (d) $m_{f,a}$=17.5, (e) $m_{f,a}$=18, (f) $m_{f,a}$=24.

the asynchronous PS-PWM is allowed, and the switching frequency is fixed to its maximum available value of 750 Hz. When n>500 rpm, the Synch PS-PWM is enabled, and the switching frequency is varied over the speed range depending on the fundamental frequency according to equation (8). In detail, the transition between two values of m_f^* is managed by imposing that when the upper frequency bound is reached, m_f^* must be decreased according to (8) until the new switching frequency value is lower than the lower frequency bound. The obtained switching frequency-motor speed pattern is shown in Fig. 4 and identified by the dotted brown line. Specifically, the dotted brown line represents the ideal relationship between switching frequency and motor speed. However, this trend is not directly implemented in the closed-loop control, as operating near a transition point of m_f^* can determine its oscillation between two adjacent values due to the speed ripple and the measurement noise, potentially leading to system instability. For this reason, a hysteresis band of 60 rpm is adopted to avoid instability issues near a transition point of m_f^*, and the dotted brown line trend is split into two trends, identified by blue and red continuous lines, which are valid for positive and negative accelerations, respectively. As a way of example, supposing to perform an acceleration from 1500 rpm to 2500 rpm, the theoretical value of motor speed that triggers the transition from m_f^*=7.5 to m_f^*=4.5 is 2000 rpm. However, the effective transition occurs at 2030 rpm due to the hysteresis. On the contrary, during a 2500 to 1500 rpm deceleration, the effective transition from m_f^*=4.5 to m_f^*=7.5 occurs at 1970 rpm.

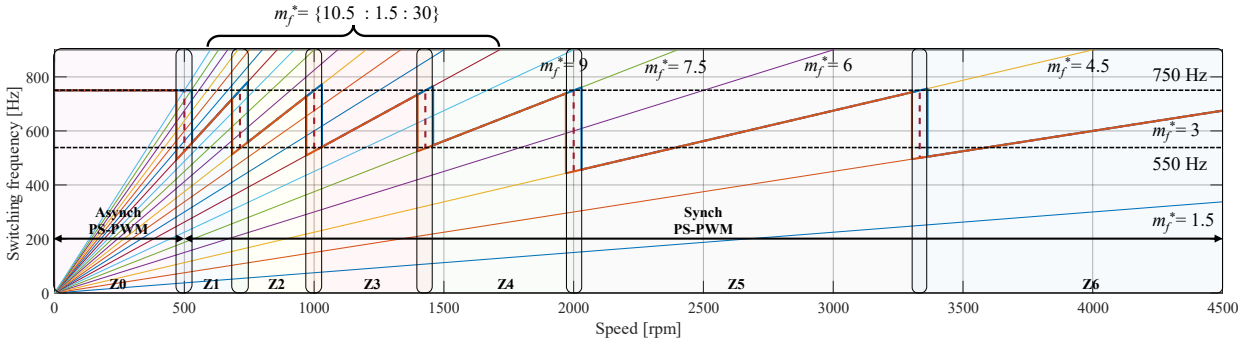

Fig. 4: Switching frequency – motor speed pattern for 3P-5L-CHBMI-fed PMSM Drive.

B. *Synch PS-PWM-based FOC Implementation*

The switching frequency-motor speed pattern discussed so far is designed and computed offline. Then, it is implemented into a Field Oriented Control strategy according to the block scheme reported in Fig. 5.

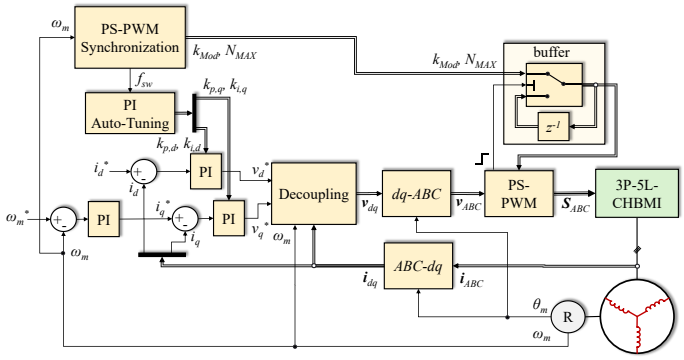

Fig. 5. Field Oriented Control with Synch PS-PWM block scheme.

The Synch-PS-PWM-driven FOC is experimentally implemented on the System on Module (SoM) sbRIO 9651 controller by National Instrument. It is based on Xilinx Zynq 7000 System on a Chip (SoC) and consists of a Xilinx Zynq FPGA and a ARM Cortex A9 DSP modules. Both modules can be programmed independently in the LabVIEW environment. SoM sbRIO 9651 is equipped on a Power Electronics and Drives (PED) Board, for fast prototyping purposes. According to Fig. 5, the PS-PWM synchronization block is devoted to computing the switching frequency and related modulation parameters such that the synchronization between the carriers frequency and the fundamental frequency is reached according to (8). The modulation parameters include the maximum counting value N_{MAX} of the up-down counters implemented for the generation of the carrier signals, and the related modulating signals scaling factor k_{Mod}. With this aim, the IPMSM drive speed operative area is further split into seven zones, named Zone0, Zone1, …, Zone6, as it is shown in Fig. 4. In detail, Zone0 corresponds to the speed range where the asynchronous PS-PWM is allowed. Remaining zones fall within the Synch-PS-PWM working area: each zone is delimited by two adjacent transitions of m_f^* and contains a linear f_{sw}-n trend, whose slope is correlated to m_f^*. Thus, the main features of each zone, i.e., the zone indicator value, the fundamental frequency zone delimiters (including the hysterisis bounds), and the corresponding value of m_f^* are stored in a Look Up Table (LUT) and selected online depending on the current value of the fundamental frequency. Fig. 6 shows operations inside the PS-PWM synchronization block implemented in the LabVIEW FPGA target.

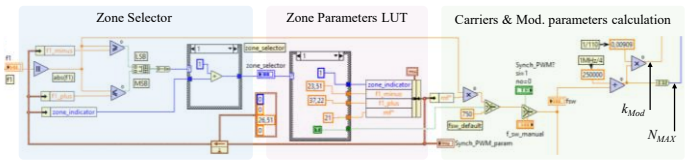

Fig. 6. Operations inside the PS-PWM synchronization block implemented in the LabVIEW FPGA Target.

In detail, the current fundamental frequency value is compared to the fundamental frequency zone delimiters and when it exceeds the zone delimiters, the zone selector variable is increased or decreased, depending on whether the superior or inferior limit has been exceeded. Once the zone is defined, the value of m_f^* is adopted to compute online the switching frequency f_{sw} and related modulation parameters N_{MAX} and k_{Mod}. It is crucial to update the maximum and minimum counting values of the up-down counters and the related modulating signal scaling factor to maintain the proper carrier phase shift and the proper amplitude modulation index. In detail, updating the up-down counters in a random instant would result in the loss of the desired phase shift, while updating the carriers amplitude and modulating signals asynchronously would result in an undesired variation of the amplitude modulation index, which would produce a wrong control action and consequently current spikes. To face this issues and to make the transition between m_f^* values transparent to the control algorithm, the novel up-down counters parameters and scaling factor are buffered and updated into the modulation stage only once per carriers period, i.e., when two carriers pass from zero and the others reach their maximum and minimum value respectively, as shown in Fig. 7. To avoid varying the control sampling frequency with the switching frequency, the former is kept constant and equal to 10 kHz, i.e., much higher than the apparent switching frequency. Moreover, current sampling and control action updates are carried out at a random instant of the carriers period, as shown in Fig. 7. Consequently, the current ripple is sampled. However, this is an implementation comprise which will not significantly affect steady state and dynamic performance, as will be shown in Section V.

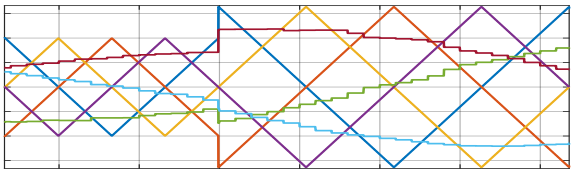

Fig. 7. Example of synchronous updating of the carriers maximum counting value N_{MAX} and modulating signals scaling factor k_{Mod}.

C. *PI regulators Auto-Tuning strategy*

Since the Synch PS-PWM strategy determines a switching frequency variation depending on the motor speed, an auto-tuning strategy for PI regulators is recommended to guarantee the best steady-state and dynamic performance under every working condition. With this aim, a zero-pole cancellation strategy is adopted for the current control loop. The speed control loop is tuned by a trial-and-error fashion, and proportional and integral gains are kept constant. The d and q current control channels are summarized through the block scheme reported in Fig. 8.

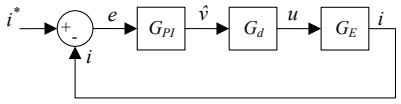

Fig. 8. Inner current control loop block scheme.

It consists of three transfer functions, G_{PI}, G_d, and G_E, that model the PI controller action, the delay due to the modulation stage, and the PMSM electric phenomena, respectively. In the Laplace domain, G_{PI}, G_d, and G_E are expressed as:

$$G_{PI} = \frac{\hat{v}}{e} = k_p + \frac{k_i}{s} = k_p\left(1 + \frac{1}{T_i s}\right) \tag{9}$$

$$G_d = \frac{u}{\hat{v}} = \frac{1}{1 + T_d s} \tag{10}$$

$$G_E = \frac{i}{u} = \frac{1}{R + Ls} \tag{11}$$

The modulation delay introduced by the PS-PWM strategy is correlated to the apparent switching frequency according to (4) and it is expressed as follows:

$$T_d = 1.5\frac{T_{PWM}}{n_l - 1} \tag{12}$$

Where T_{PWM} is the carriers period. For a 3P-5L CHBMI, T_d=3/8T_{PWM}. By imposing that the integral time constant T_i coincides with the electric time constant T_E, it is possible to realize a zero-pole cancellation such that the closed-loop transfer function W_E can be simplified to a second-order one:

$$W_E = \frac{i}{i^*} = \frac{\frac{k_p}{LT_d}}{s^2 + \frac{1}{T_d}s + \frac{k_p}{LT_d}} \tag{13}$$

Expressing (13) in standard form and imposing a damping coefficient ζ_E=0.707, it is possible to determine the natural pulsation $\omega_{n,E}$, and the proportional and integral gains k_p and k_i as follows:

$$\omega_{n,E} = \frac{4}{3}\sqrt{2} f_{sw} \tag{14}$$

$$k_p = \frac{4}{3} f_{sw} L \tag{15}$$

$$k_i = \frac{k_p}{T_i} = \frac{4}{3} f_{sw} R \tag{16}$$

(15) and (16) represent very simple and low-computational-cost PI auto-tuning equations, which only depend on the IPMSM parameters and on the switching frequency. They are implemented in the PI auto-tuning block reported in Fig. 5.

IV. Test Bench

The test bench is shown in Fig. 9. The AC drive has already been described in Section III. Some extra details are reported in [15].

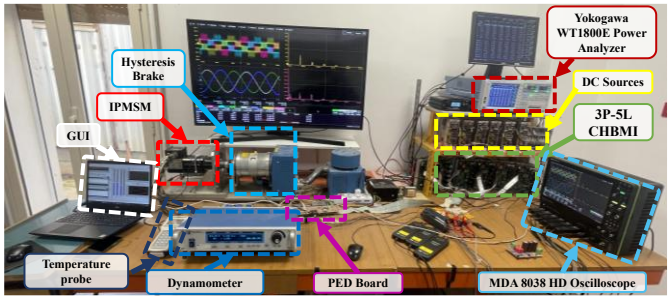

Fig. 9. Test bench at the SDESLAB of the University of Palermo.

Phase voltage and currents are measured through a Teledyne LeCroy MDA 8038HD oscilloscope with a sampling frequency of 1 MHz and over an observation window of 1 s, guaranteeing a frequency resolution of 1 Hz and the synchronous sampling condition. It is equipped with three high-voltage differential probes, Teledyne Lecroy HVD3106A 1 kV, 120 MHz, and three high-sensitivity current probes Teledyne Lecroy CP030A AC/DC, 30 A rms, 50 MHz. Magtrol HD-715-8NA hysteresis brake allows for applying the desired load torque to the system, and it can be controlled through the DSP6001 dynamometer.

V. Experimental Validation

In this section, the proposed Synch PS-PWM-based FOC strategy is validated through experimental analysis, both in steady state and dynamic working conditions. Regarding steady state analysis, CHBMI-fed IPMSM drive performance are investigated at two working points identified by two values of rotor speed, i.e., 2000 rpm and 3000 rpm, and rated load torque of 1.8 Nm. To validate the simulation results presented in Section II, the proposed Synch-PS-PWM strategy is compared with the PS-PWM strategy in asynchronous conditions. Phase voltages and currents are measured according to the discussion carried out in Section IV. Regarding dynamic working condition analysis, a 0-3000 rpm acceleration at no-load is performed. In this case, current, speed, and switching frequency trends are recorded through the control board at the control sampling frequency of 10 kHz.

A. Steady-state analysis

Fig. 10 and Fig. 11 show the comparison between phase voltage and current trends both in the time and frequency domains when the load torque is equal to 1.8 Nm, and when the rotor speed is 2000 rpm and 3000 rpm, respectively. To validate the simulation results presented in Section II, three values of $m_{f,a}$ are adopted per each investigated working point, i.e., $m_{f,a}$ =29, $m_{f,a}$ =29.5, and $m_{f,a}$=30 (corresponding to m_f =7.25, m_f =7.375, and m_f =7.5, respectively) when n=2000 rpm, and $m_{f,a}$ =17, $m_{f,a}$ =17.5, and $m_{f,a}$=18 (corresponding to m_f =4.25, m_f =4.375, and m_f =4.5, respectively) when n=3000 rpm. Looking at the voltage trends, it can be stated that experimental analysis confirms the simulation results. In detail, an odd integer value of $m_{f,a}$ (i.e., 29 and 17) produces both odd and even harmonics in the spectra, with the dominant group clustered around the apparent switching frequency being even harmonics; a non-integer value of $m_{f,a}$ (i.e., 29.5 and 17.5) produces both odd and even harmonics that are present in every harmonics cluster. It must be underlined that the lack of three-phase symmetry is less evident in experimental results since spectra related to the three phases are almost superimposed in every condition. Some similar considerations can be carried out regarding the current trends and related spectra. Thus, to quantify the benefits related to the adoption of a synchronous modulation strategy, the current Total Harmonic Distortion (THD) is investigated. In detail, TABLE III shows a comparison between the current THD in the investigated working points and for every considered frequency modulation index. In both cases, it can be noted that the Synch-PS-PWM strategy guarantees the lowest current THD, equal to 3.13% and 6.05% when n=2000 rpm and n=3000 rpm, respectively.

TABLE III. Current THD as a function of the motor speed and of the frequency modulation index.

n [rpm]	2000			3000		
m_f [-]	7.25	7.375	7.5	4.25	4.375	4.5
THD_i [%]	3.42	3.40	3.13	6.51	6.37	6.05

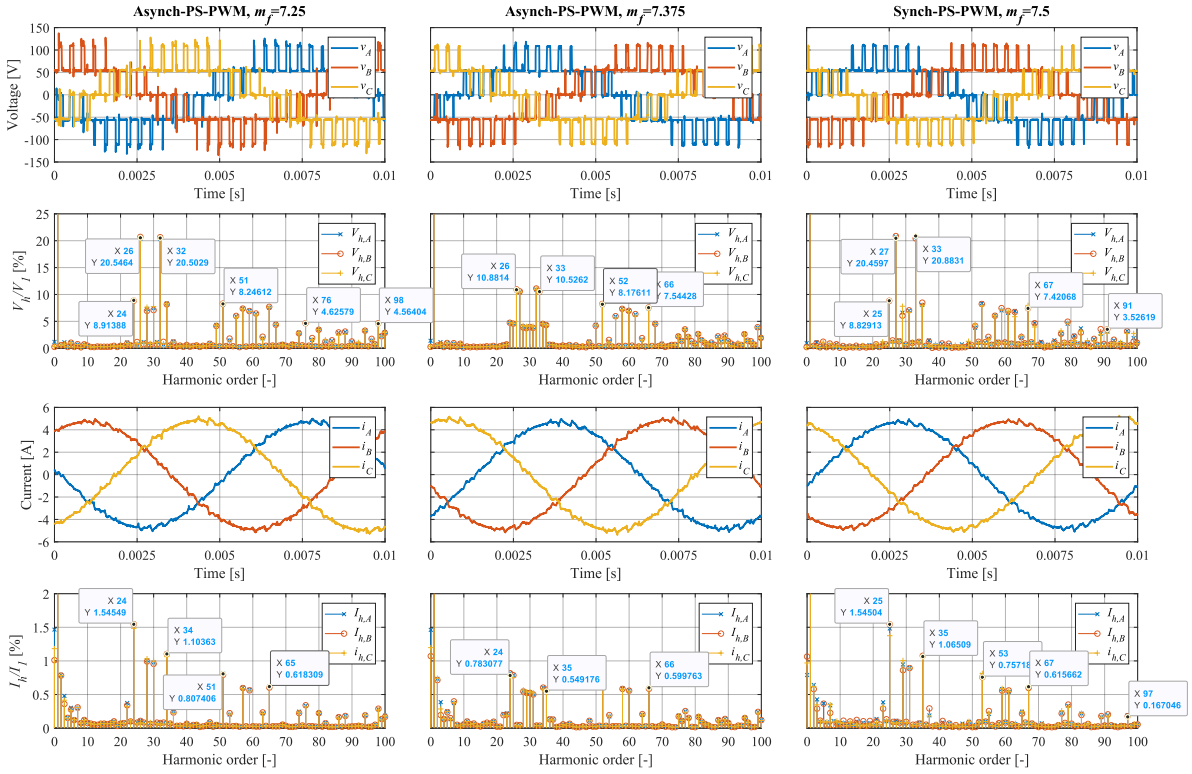

Fig. 10. Comparison between phase voltage and current trends both in the time and frequency domain under synchronous and asynchronous modulation conditions: n=2000 rpm, T=1.8 Nm, (a) $m_{f,a}$=29, m_f=7.25, (b) $m_{f,a}$=29.5, m_f=7.375, (c) $m_{f,a}$=30, m_f=7.5.

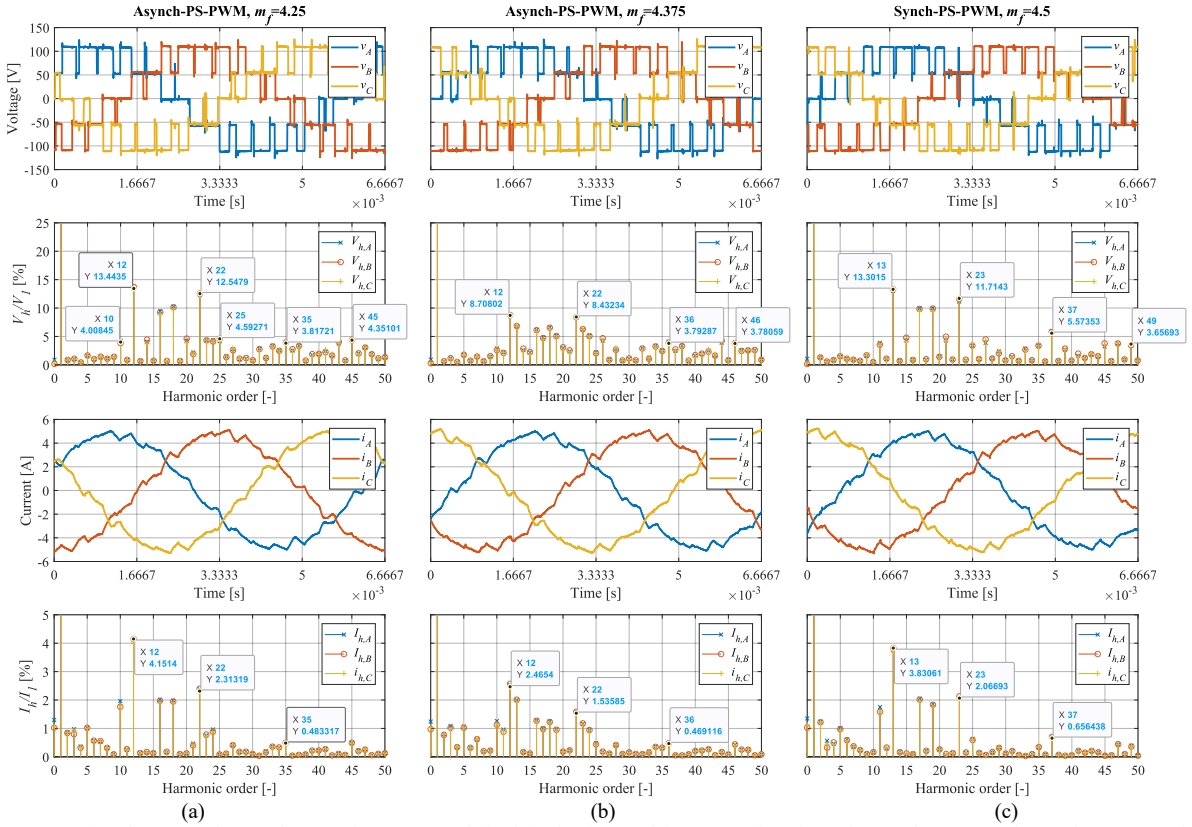

Fig. 11. Comparison between phase voltage and current trends both in the time and frequency domain under synchronous and asynchronous modulation conditions: n=3000 rpm, T=1.8 Nm, (a) $m_{f,a}$=17, m_f=4.25, (b) $m_{f,a}$=17.5, m_f=4.375, (c) $m_{f,a}$=18, m_f=4.5.

B. *Dynamic analysis*

Fig. 12 shows the speed, currents, and switching frequency trends determined by the Synch-PS-PWM-based FOC during a 0-3000 rpm acceleration at no-load conditions. It can be noted that the IPMSM drive exhibits good dynamic performance, with a speed transient that ends in about 0.4 s with an overshoot lower than 10%, and a *q* current transient that ends in about 8 ms without overshoot. Moreover, although the switching frequency and the PI regulator gains vary due to the speed increase, current trends show no spikes or oscillations, proving the effectiveness of the implemented control strategy.

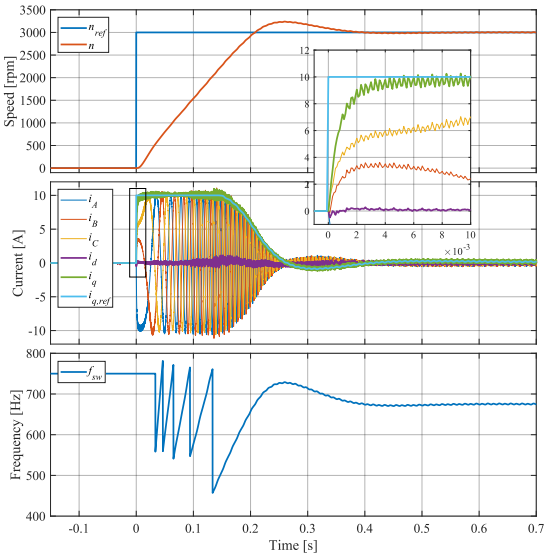

Fig. 12. Speed, *ABC* and *dq* currents, and switching frequency trends during a 0-3000 rpm acceleration at no-load conditions.

VI. Conclusions

In this work, a novel Syn-PS-PWM strategy for a 3P-5L-CHB-fed IPMSM drive is proposed. The key novelty of the proposed work deals with identifying a novel switching frequency-speed pattern that allows for maintaining voltages half-wave and three-phase symmetries even if the frequency modulation index is a fractional number. Thus, the proposed strategy allows for extending the optimal frequency modulation index range if compared to the scientific literature. The proposed Syn-PS-PWM strategy is implemented in a FOC and experimentally validated both in steady state and dynamic working conditions.

Acknowledgment

This work was supported in part by European Union—NextGenerationEU-National Sustainable Mobility Center CN00000023, Italian Ministry of University and Research Decree n. 1033—17/06/2022, Spoke 3, 12, CUP B73C22000760001, in part by the Prin 2022-Settore/Ambito di intervento: PE7 Enhanced Energy-Saving Powertrains for Freight E-Transportation (ESPFET) under Grant PRJ-0962-CUP B53D23002440006. The authors would like to acknowledge that this work was carried out in the following laboratories: Sustainable Development and Energy Saving laboratory (SDESLab), Rapid Prototyping Laboratory (RPLab), Laboratory of Electrical Applications (LEAP) at the Department f Engineering, Building no.9, University of Palermo, Italy.

References

[1] F. J. T. E. Ferreira and A. T. de Almeida, "Reducing Energy Costs in Electric-Motor-Driven Systems: Savings Through Output Power Reduction and Energy Regeneration," in IEEE Industry Applications Magazine, vol. 24, no. 1, pp. 84-97, Jan.-Feb. 2018.

[2] J. Holtz and X. Qi, "Optimal Control of Medium-Voltage Drives—An Overview," in *IEEE Transactions on Industrial Electronics*, vol. 60, no. 12, pp. 5472-5481, Dec. 2013.

[3] H. Abu-Rub, J. Holtz, J. Rodriguez and G. Baoming, "Medium-Voltage Multilevel Converters—State of the Art, Challenges, and Requirements in Industrial Applications," in *IEEE Transactions on Industrial Electronics*, vol. 57, no. 8, pp. 2581-2596, Aug. 2010.

[4] B. Singh, R. Kumar and P. Kant, "Adjustable Speed Induction Motor Drive Fed by 13-Level Cascaded Inverter and 54-Pulse Converter," in *IEEE Transactions on Industry Applications*, vol. 58, no. 1, pp. 890-900, Jan.-Feb. 2022.

[5] A. Marzoughi, R. Burgos and D. Boroyevich, "Investigating Impact of Emerging Medium-Voltage SiC MOSFETs on Medium-Voltage High-Power Industrial Motor Drives," in IEEE Journal of Emerging and Selected Topics in Power Electronics, vol. 7, no. 2, pp. 1371-1387, June 2019.

[6] B. P. McGrath and D. G. Holmes, "Multicarrier PWM strategies for multilevel inverters," in IEEE Transactions on Industrial Electronics, vol. 49, no. 4, pp. 858-867, Aug. 2002.

[7] J. I. Leon, S. Kouro, L. G. Franquelo, J. Rodriguez and B. Wu, "The Essential Role and the Continuous Evolution of Modulation Techniques for Voltage-Source Inverters in the Past, Present, and Future Power Electronics," in IEEE Transactions on Industrial Electronics, vol. 63, no. 5, pp. 2688-2701, May 2016.

[8] E. -J. Lee, S. -M. Kim and K. -B. Lee, "Modified Phase-Shifted PWM Scheme for Reliability Improvement in Cascaded H-Bridge Multilevel Inverters," in IEEE Access, vol. 8, pp. 78130-78139, 2020.

[9] A. Edpuganti and A. K. Rathore, "A Survey of Low Switching Frequency Modulation Techniques for Medium-Voltage Multilevel Converters," in *IEEE Transactions on Industry Applications*, vol. 51, no. 5, pp. 4212-4228, Sept.-Oct. 2015.

[10] L. Xiao, J. Li, Y. Xiong, J. Chen and H. Gao, "Strategy and Implementation of Harmonic-Reduced Synchronized SVPWM for High-Power Traction Machine Drives," in *IEEE Transactions on Power Electronics*, vol. 35, no. 11, pp. 12457-12471, Nov. 2020.

[11] J. -S. Kim, D. -H. Kim, J. -H. Lee, Y. -S. Song and J. -S. Lee, "Synchronous PWM Pulse Number Selection for High-Efficiency Drive of Propulsion System," *IECON 2023- 49th Annual Conference of the IEEE Industrial Electronics Society*, Singapore, Singapore, 2023, pp. 1-5.

[12] S. Furutani and S. Doki, "Synchronous PWM Method Considering Motor Current Control for 2Level-3Phase Inverter," *2022 25th International Conference on Electrical Machines and Systems (ICEMS)*, Chiang Mai, Thailand, 2022, pp. 1-6.

[13] Y. Li, Y. Wang and B. Q. Li, "Generalized Theory of Phase-Shifted Carrier PWM for Cascaded H-Bridge Converters and Modular Multilevel Converters," in *IEEE Journal of Emerging and Selected Topics in Power Electronics*, vol. 4, no. 2, pp. 589-605, June 2016.

[14] G. Schettino, A. O. Di Tommaso, R. Miceli, C. Nevoloso, G. Scaglione and F. Viola, "Dead-Time Impact on the Harmonic Distortion and Conversion Efficiency in a Three-Phase Five-Level Cascaded H-Bridge Inverter: Mathematical Formulation and Experimental Analysis," in *IEEE Access*, vol. 11, pp. 32399-32426, 2023.

[15] C. Nevoloso *et al*., "On the Inadequacy of IEC 60034-2-3 and IEC 60034-30-2 Standards for Power Losses, Efficiency and Energy Class Evaluation in PWM Multilevel Inverter-Driven PMSM," in *IEEE Open Journal of the Industrial Electronics Society*, vol. 6, pp. 962-981, 2025.

[16] S. K. Sahoo and T. Bhattacharya, "Phase-Shifted Carrier-Based Synchronized Sinusoidal PWM Techniques for a Cascaded H-Bridge Multilevel Inverter," in *IEEE Transactions on Power Electronics*, vol. 33, no. 1, pp. 513-524, Jan. 2018.